Dynamic imaging of transient bubbles generated by femtosecond irradiation of plasmonic nanoparticles in suspensions and cell environment

Christos Boutopoulos*, Matthieu Fortin-Deschênes, Eric Bergeron, Michel Meunier
Laser Processing and Plasmonics Laboratory, Department of Engineering Physics, Ecole Polytechnique de Montreal, CP. 6079 Succ. Centre-ville, Montreal, H3C 3A7 Quebec, Canada

ABSTRACT

Femtosecond (fs) laser generation of submicron bubbles around plasmonic nanoparticles (NPs) plays a key role in advanced laser nanosurgery applications such as cell membrane perforation and cell transfection. In this context, we have developed a pump-probe shadowgraphic ultrafast imaging technique capable of tracking transient bubbles generated by fs irradiation (λ =800 nm, τ = 45 fs) of: (a) plasmonic NPs in suspensions and (b) plasmonic NPs attached to cells. The laser fluence was systematically varied from 100 mJ/cm^2 to 500 mJ/cm^2 to study the effect on the bubble dynamics generated around 100 nm gold NPs (Au NPs). The plasmonic bubble (PB) generation threshold as well as the NPs deformation threshold were defined. Dark field (DF) imaging and scanning electron microscopy (SEM) revealed NP clustering when 100 nm bare Au NPs were incubated with a cancer cell culture. NP clustering was correlated with PB generation using a combined pump-probe and DF imaging approach. The clustering effect resulted in a significant 4-times decrease to the PB generation threshold compared to single NPs. The clustering effect was further investigated by evaluating bare and polyethylene glycol (PEG) functionalized NPs in terms of PB generation efficiency.

Keywords: cavitation bubbles, cell perforation, dynamic imaging, femtosecond laser, laser nanosurgery, nanoparticle cluster, plasmonic nanoparticle, bioplasmonics.

1. INTRODUCTION

Plasmonic bubble (PB) detection and more importantly PB *in-situ* monitoring allows for understanding cell membrane perforation mechanisms as well as for nanosurgery processing optimization. Therefore, due to their crucial role in cell nanosurgery, PB generation around pulsed laser exited plasmonic NPs is receiving growing interest by several research groups[1–4]. Due to their transient and confined nature, PB studies require development of detection methods with nanoscale temporal and spatial resolution.

In the topic of plasmonic NP enhanced laser nanosurgery, there are several aspects related to processing optimization and mechanisms understanding that remain unclear. NP fragmentation is one of the more important issues. Indeed, small NP fragments (< 2 nm) have been reported to cause necrosis and mitochondrial damage on many cell lines[5]. Therefore, NP fragmentation has to be avoided in order to eliminate any undesirable side effect of the process. NP functionalization is also a well-known strategy for increasing their biocompatibility. Indeed, *in-vivo* studies have shown that poly(ethylene glycol) (PEG) functionalization protects gold NPs (Au NPs) from an immune system response[6].

Herein, we propose and apply a dynamic imaging method for studying PB generation under femtosecond (fs) laser irradiation of plasmonic NPs. We focus on a single NP approach to define PB generation and NP fragmentation thresholds for a 100 nm Au NP suspensions. The effect of PEG functionalization of Au NPs on PB generation is also studied. Finally, PB imaging is performed on cancer cell samples to study the NP clustering effect on PB dynamics.

2. MATERIALS AND METHODS

2.1 Dynamic imaging

The fast dynamics, involved in PB generation and evolution, could not be captured by conventional high speed cameras. Therefore, we used an ultrafast pump-probe shadowgraphic imaging system for our study. A Ti:Sapphire laser (6

* e-mail: christos.boutopoulos@polymtl.ca; tel. : +1 5143405121 ext. 7455

Frontiers in Ultrafast Optics: Biomedical, Scientific, and Industrial Applications XIV, edited by Alexander Heisterkamp, Peter R. Herman, Michel Meunier, Stefan Nolte, Proc. of SPIE Vol. 8972, 897208
 · doi: 10.1117/12.2039951

mJ/pulse, 45 fs, 800 nm, 1 to 1000 Hz, Spitfire from Spectra-Physics) was used as the pump laser to produce the PBs and a Nd:YAG laser (0.4 J/pulse, 6 ns, 532 nm, 10Hz, Brillant from Quantel) was used as the probe laser. The delay between the pump-probe pulses was adjusted (0 to 200 ns) using two delay generators to synchronize the lasers at 10 Hz. The probe pulses (532 nm, 6 ns) were used to pump a container with a Rhodamine 6G dye. This resulted in PB imaging with incoherent light (590 nm, ~ 6 ns).

Approximately 30 µL of Au NPs solution diluted in phosphate-buffered saline (PBS, Sigma-Aldrich) was placed in a glass bottom petri dish with a cover slip covering the drop to counter the lens effect produced by the curve of the drop as shown in Figure 1. The petri dish was placed under a microscope equipped with a 50x long working distance objective. An IMI Teck IMB-17FT CCD camera was used to capture the PBs generation. A dark field (DF) imaging function was used in addition to the pump-probe system in order to either locate NPs in a cell sample or track NPs Brownian motion.

The pump beam was slightly focused at the imaging plane of the pump-probe and DF systems using a converging lens (f = 750 mm). A Gaussian beam profile was measured with a spot diameter of 0.5 mm (defined at $1/e^2$). We have considered the maximum fluence (2-times the average fluence) for our analysis since we performed imaging at the central part of the beam.

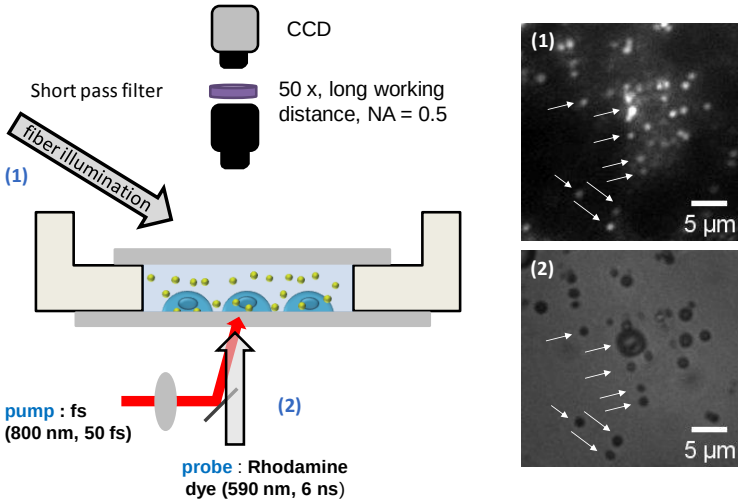

Figure 1: Experimental setup showing a typical sample under the two imaging systems. The dark field (DF) imaging system allows for NP detection and dynamic tracking. (1) indicates the DF system as well as a typical DF image of NPs attached to a cancer cell. The pump-probe shadowgraphic imaging system allows for PB detection with sub-micron spatial resolution and ~ 1 ns temporal resolution. (2) indicates the pump-probe system as well as a typical pump-probe image of PBs generated by laser irradiation of NPs attached to a cancer cell. The arrows indicate colocalization of NP and PB signals.

2.2 Single NP tracking

Changing the pump-probe delay from pulse to pulse (i.e., corresponds to successive frames of the camera) resulted in imaging of successive PBs generated by the same NP at different stages of its lifetime. Therefore, PB dynamics were investigated by analysing the different images. Experiments of PB imaging were performed as follows: (a) NPs were first tracked in DF imaging to identify single NP motion (see below) (b) PBs generated around a single NP were studied by changing the imaging system to the pump-probe mode.

Bare NPs in a liquid suspension tend to bind together and form clusters due to electrostatic interactions. Therefore, fs irradiation will produce a mixture of PB generated from either single NPs or clusters of NPs. We have studied the Brownian motion of the NPs in our samples to ensure single NP tracking. Brownian motion is the random motion of particles in a liquid due to the collisions between the molecules of the liquid and the moving particle. The diameter of a particle can be found by the following Brownian motion characteristic equation:

$$d = \frac{2RT\tau}{3\pi\eta N_A \overline{X^2}} \quad (1)$$

Where R is the gas constant, T is the temperature, N_A is the Avogadro constant, η is the viscosity of the liquid, $\overline{\chi^2}$ is the mean squared displacement for the time τ. In order to distinguish the clusters from the single NPs, their motion was tracked in DF mode and compared to the one predicted by Brownian motion equation. PB images were processed only for NPs that have been confirmed as single ones by using equation 1.

2.3 NP samples

Citrate-capped Au NPs were purchased from spi (44.4 μg/mL, diameter 100 nm, spi, 4804-AB, West Chester, PA) and stored at 4°C in the dark to minimize photoinduced oxidation. Au NPs (450 μL) were functionalized with an aqueous solution of methoxy PEG thiol (OMe-PEG-SH, 2kDa, 0.1 mg/mL, 50 μL Sigma-Aldrich) during 1h at 4°C by using the strong covalent gold-sulfur bond[7]. Excess of OMe-PEG-SH was eliminated by centrifugation at 5000 rpm during 2 min. The supernatant was removed and replaced with phenol-free Dulbecco's modified Eagle's medium (DMEM, Life Technologies) containing 4.5 g/L *D*-glucose, 584 mg/L *L*-glutamine and 110 mg/L sodium pyruvate and supplemented with 100 units/mL penicillin and 100 μg/mL streptomycin.

2.4 Cell culturing and cell sample preparation

MDA-MB-231 human breast cancer cells were seeded onto glass bottom dishes and grown in Dulbecco's modified Eagle's medium (DMEM, containing 4.5 g/L *D*-glucose, 584 mg/L *L*-glutamine and 110 mg/L sodium pyruvate) supplemented with 10% foetal bovine serum (FBS, Life Technologies), 100 units/mL penicillin and 100 μg/mL streptomycin in a humidified incubator at 37 °C under a 5% CO_2 atmosphere. When cells reached 80% confluence, they were washed once with PBS. The cells were then incubated with 8.2 μg/mL 100 nm Au NPs in serum-free medium during 2-4 h in the 37 °C prior to either PB detection or SEM observations.

2.5 Scanning electron microscopy (SEM)

Cells grown as above were incubated with Au NPs at 8.2 μg/mL during 4h. Then, cells were washed three times with PBS, fixed in 5% glutaraldehyde/95% PBS for 30 min, then incubated in 5% glutaraldehyde/95% water for 30 min. The samples were then washed 3 times with distilled water and dried overnight under a fume hood. Samples were coated with a 5 nm uniform gold layer (Agar manual sputter coater, Marivac, Montréal, QC). SEM images were captured in conventional high-vacuum mode on an ESEM Quanta 200 FEG (FEI, Hillsboro, OR) at 20kV, 60.000X and a working distance of 12-15 mm.

3. RESULTS

3.1 Detection of PB around single NPs

In order to evaluate the dynamic imaging method, the initial experimental work was oriented toward the detection of multiple PB generated around single 100 nm bare Au NPs. As it has been discussed in the experimental part, the Brownian motion of the NPs combined with dynamic pump-probe imaging resulted in singe PB tracking. A typical example of PBs generated by single NPs under 200 mJ/cm^2 is shown in Figure 2. The various frames correspond to successive pulses (10 Hz repetition rate) at the same region of the sample. It is mentioned that pump-probe delay was set to 10 ns for this series of pictures. In this time frame, PBs have reached a sub-micron size. PB generation threshold was defined to be 145 mJ/cm^2. By changing the pump-probe delay, we observed a PB life time of about 30 - 50 ns for laser fluences ranging from 140 to 300 mJ/cm^2.

The NP deformation threshold has been also determined by monitoring *in-situ* the DF intensity in the laser irradiated area. In particular, we have monitored *in-situ* the DF intensity of various NP samples by applying a pulse to pulse alteration of the laser fluence. Figure 3 presents the normalized DF intensity integrated across the laser irradiated area of the various Au NP samples. The DF intensity plateau at low laser fluence is indicative of intact NPs while the plateau at high laser fluence is indicative of NP elimination. The laser fluence range resulting in progressive DF decrease indicates partial NP fragmentation (size reduction) and/or NP elimination. Considering the NP fragmentation threshold (~ 280 mJ/cm^2) as well as the PB generation threshold (145 mJ/cm^2), we can define their ratio (~ 1.9) as a measure of effective processing window range.

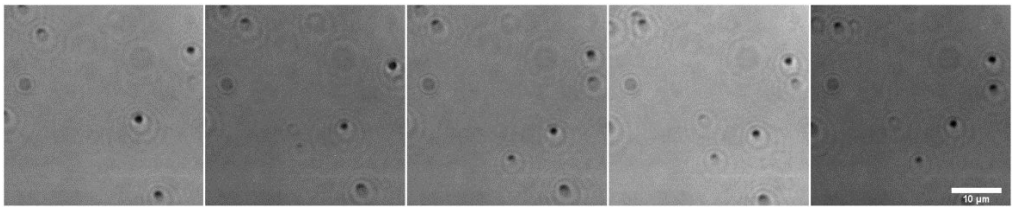

Figure 2: A series of pump-probe images of submicron plasmonic bubbles (PBs) generated by laser irradiation of 100 nm Au NPs at 10 Hz. Pumb-probe delay was set at 10 ns (i.e., PBs were captured 10 ns after their generation)

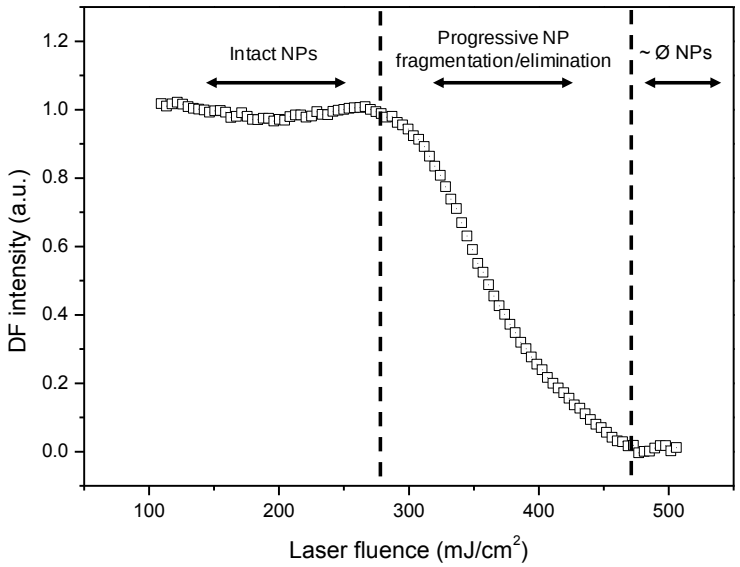

Figure 3: Normalized dark field (DF) intensity integrated across the laser irradiated area of the various 100 nm Au NP samples. The intensity plateau at low laser fluence is indicative of intact NPs while the plateau at high laser fluence is indicative of NP elimination. Laser fluence range resulting in progressive DF decrease indicates partial NP fragmentation (size reduction) and/or elimination. The filled square indicates the estimation for the NP deformation threshold.

3.2 The effect of PEG functionalization of NPs on PB generation

We have used two different approaches to study the effect of PEG functionalization of Au NPs on PB generation. In the first approach, PB generation was studied by dynamic imaging in the middle part of the sample container. By using this experimental methodology, PB tracking around single NPs was ensured. In the second approach, PB generation was studied in the bottom of the sample container (i.e, glass cover slip) where clusters of NPs were formed due to NP precipitation. The results for both approaches are summarized in Table 1. For bare NPs, we observed PB generation threshold of 145 mJ/cm^2 and 35 mJ/cm^2 for single NP and clustered NPs, respectively. For PEG-NP, we observed PB generation threshold of 155 mJ/cm^2 and 70 mJ/cm^2 for single NP and clustered NPs, respectively. In general, NP clustering results in a decrease to the required energy for PB generation compared to single NPs. This is due to the formation of the so-called "hot-spots" (i.e., regions with enhanced field amplification) within the assembly of the NP clusters.

We have found a slight higher PB generation threshold (155 mJ/cm^2) for bare Au NPs compared to PEG-Au NPs (145 mJ/cm^2). The PEG effect on the PB generation threshold can be attributed to the relative lower near field amplification around the PEG-Au NPs compared to bare Au NPs. Indeed, we have calculated 5 % less near field amplification when Au NPs were surrounded with a 4 nm layer (i.e., typical PEG layer thickness) of PEG in our calculations. A more dominant effect of the PEG functionalization can be observed when comparing PB generated by clusters of NPs (70 vs 35 mJ/cm^2). PEG-Au NP clusters require two times more energy to generate a PB compared to Au NP clusters. This

result could be explained if we consider PEG effect on NPs clustering. In general, PEG functionalization decreases the NP clustering effect; therefore, the number of "hot spots" is probably less for clustered PEG-NPs compared to clustered bare NPs. In addition, the minimum inter-particle distance is expected to be limited to 8 nm for PEG-NP clusters due to the 4 nm PEG layer thickness. This results to a significant decrease of the maximum field amplification per NP dimer and/or cluster for a certain incident pulse energy[8].

Table 1: Plasmonic bubble (PB) detection thresholds for Au NPs and PEG-Au NPs

NP	PB detection threshold for single NPs (mJ/cm^2)	PB detection threshold for NP clusters (mJ/cm^2)
100 nm Au NPs	145	35
100 nm PEG-Au NPs	155	70

3.3 PB detection in cell environment

In a typical NP-assisted cell membrane perforation experiment[9], cell samples are incubated with plasmonic NP for a time period ranging from 30 min to few hours. We have reproduced a typical membrane perforation experiment using MDA-MB-231 human breast cancer cells and 100 nm Au NPs. Using the pump-probe methodology, we have detected PB around the vicinity of the cells for laser irradiation of 200 mJ/cm^2 (defined as 2-times the average fluence) at a 10 ns pump-probe delay. Figure 4 shows typical figures of a cancer cell under DF, pump-probe and SEM observation. DF microscopy reveals several bright spots on the surface of the cell and around, indicative of NPs and NP clusters (Figure 4a). Following the first irradiation pulse, a plethora of PBs was detected in the sample at a 10 ns pump-probe delay (Figure 4b). The size of the PBs ranged from 1 to 5 μm, indicating NP clustering in the sample. Indeed, NP clusters form "hot spots" of enhanced field enhancement[10], which could result in the generation of larger PBs. On the other hand, according to section 3.1, sub-micron PBs could be associated to single NPs. Figure 4c demonstrates a characteristic break of the NP clusters following 10 successive laser pulses. NP clusters breaking results in the diffusion of the single NPs. As a result, several sub-micron bubbles can be detected around the major clustering regions of our sample. A typical SEM picture of a cancer cell surface, following 3h incubation with PEG Au NPs, is shown in Figure 4d.

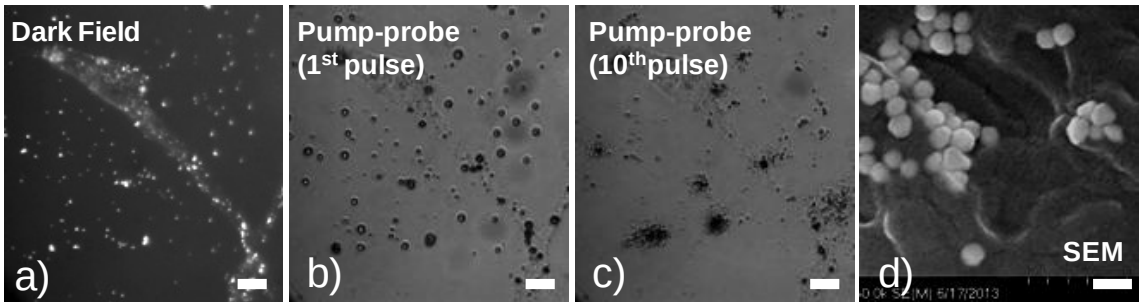

Figure 4: (a) Dark field (DF) image of a cancer cell after 2h incubation with 100 nm Au NPs (b) Pump-probe image (10 ns delay) of PBs generated by the first laser pulse at 200 mJ/cm^2 (c) Pump-probe image (10 ns delay) of PBs generated by the 10th laser pulse (d) An indicative SEM picture of the surface of a cancer cell surface following the 3h incubation with 8.2 μg/mL 100 nm PEG Au NPs . Scale bar is 10 μm for (a),(b) and (c), 200 nm for (d).

4. CONCLUSION

We have applied a dynamic and ultrafast imaging method to study PB generation in NP suspensions and cell samples following 800 nm fs laser irradiation. The PB generation has been studied in a single NP approach using a combined DF and pump-probe imaging approach.

PEG-Au 100 nm NP suspensions and bare Au NP suspensions were compared in terms of PB generation efficiency. We observed a small influence of the PEG functionalization on PB generation from single NPs. In contrary, PEG functionalization results in a significant 2-times increase to the PB generation threshold from clustered NPs. We mainly attribute this effect to the increased inter-particle distance in PEG-NP clusters compared to bare NP clusters. We have

also observed a smaller number of NPs in PEG-NP clusters compared to bare NP clusters, which could have cause threshold difference as well.

Finally, we observed PB generated in a cancer cell sample after 2h incubation with 100 nm NPs. NP clustering effect was observed with DF, pump-probe and SEM observations. PB generation from clusters occurred in significant lower laser fluence compared to single NPs (i.e., 35 vs 145 mJ/cm^2). PB generated by NP clusters grown up to 5 μm in 10 ns, while PB generated by single NPs expanded to a sub-micron size in the same time period.

Our results indicate that depending on the desired bio-application, PB dynamics could be controlled by selecting the optimum NP size or more importantly by mastering NPs clustering.

Acknowledgements

C.B. and E.B. have been funded by Le Fonds de recherche du Québec under post-doctoral scholarships. The authors acknowledge financial support from the Natural Sciences and Engineering Research Council of Canada (NSERC).

REFERENCES

[1] Lukianova-Hleb, E.Y., and Lapotko, D.O., "Experimental techniques for imaging and measuring transient vapor nanobubbles," Applied Physics Letters 101(26), 264102 (2012).

[2] Lachaine, R., Boulais, E., Bourbeau, E., and Meunier, M., "Effect of pulse duration on plasmonic enhanced ultrafast laser-induced bubble generation in water," Applied Physics A 112(1), 119–122 (2012).

[3] Kotaidis, V., and Plech, A., "Cavitation dynamics on the nanoscale," Applied Physics Letters 87(21), 213102 (2005).

[4] Zharov, V.P., Mercer, K.E., Galitovskaya, E.N., and Smeltzer, M.S., "Photothermal nanotherapeutics and nanodiagnostics for selective killing of bacteria targeted with gold nanoparticles.," Biophysical journal 90(2), 619–27 (2006).

[5] Pan, Y., Leifert, A., Ruau, D., Neuss, S., Bornemann, J., Schmid, G., Brandau, W., Simon, U., and Jahnen-Dechent, W., "Gold nanoparticles of diameter 1.4 nm trigger necrosis by oxidative stress and mitochondrial damage.," Small (Weinheim an der Bergstrasse, Germany) 5(18), 2067–76 (2009).

[6] Jokerst, J., Lobovkina, T., Zare, R., and Gambhir, S., "Nanoparticle PEGylation for imaging and therapy," Nanomedicine 6(4), 715–728 (2011).

[7] Hirsch, L., Halas, N., and West, J., [Whole-Blood Immunoassay Facilitated by Gold Nanoshell-Conjugate Antibodies] , in NanoBiotechnology Protoc. 303, S. Rosenthal and D. Wright, Eds., Humana Press, 101–111 (2005).

[8] Yousif, B.B., and Samra, A.S., "Optical responses of plasmonic gold nanoantennas through numerical simulation," Journal of Nanoparticle Research 15(1), 1341 (2012).

[9] Baumgart, J., Humbert, L., Boulais, É., Lachaine, R., Lebrun, J.-J., and Meunier, M., "Off-resonance plasmonic enhanced femtosecond laser optoporation and transfection of cancer cells.," Biomaterials 33(7), 2345–50 (2012).

[10] Nedyalkov, N.N., Imamova, S., Atanasov, P. a., Tanaka, Y., and Obara, M., "Interaction between ultrashort laser pulses and gold nanoparticles: nanoheater and nanolens effect," Journal of Nanoparticle Research 13(5), 2181–2193 (2010).